Journal of
Plankton Research

academic.oup.com/plankt

J. Plankton Res. (2021) 1–17. doi:10.1093/plankt/fbab001

BLOOFINZ - Gulf of Mexico

Sinking carbon, nitrogen, and pigment flux within and beneath the euphotic zone in the oligotrophic, open-ocean Gulf of Mexico

MICHAEL R. STUKEL[1,2,*], THOMAS B. KELLY[1], MICHAEL R. LANDRY[3], KAREN E. SELPH[4] AND RASMUS SWALETHORP[3]

[1]EARTH, OCEAN AND ATMOSPHERIC SCIENCE, FLORIDA STATE UNIVERSITY, TALLAHASSEE, FL 32306, USA, [2]CENTER FOR OCEAN-ATMOSPHERIC PREDICTION STUDIES, FLORIDA STATE UNIVERSITY, TALLAHASSEE, FL 32306, USA, [3]SCRIPPS INSTITUTION OF OCEANOGRAPHY, 9500 GILMAN DR., LA JOLLA, CA 92093-0227, USA AND [4]DEPARTMENT OF OCEANOGRAPHY, UNIVERSITY OF HAWAII AT MANOA, HONOLULU, HI 96822, USA

*CORRESPONDING AUTHOR: mstukel@fsu.edu

Received October 13, 2020; editorial decision January 5, 2021; accepted January 5, 2021

Corresponding editor: John Dolan

During two cruises in the oligotrophic oceanic Gulf of Mexico, we deployed sediment traps at three depths: center of the euphotic zone (EZ) (60 m), base of the EZ (117–151 m), and in the twilight zone (231 m). Organic carbon export declined with depth from 6.4 to 4.6 to 2.4 mmol C m^{-2} d^{-1}, suggesting that net particle production was concentrated in the upper EZ. Net primary production varied from 24 to 29 mmol C m^{-2} d^{-1}, slightly more than half in the upper EZ. Export ratios varied from 11 to 25%. Trap measurements of chlorophyll and phaeopigments allowed us to quantify fluxes of fresh phytoplankton and herbivorous fecal pellets, respectively, which were both minor contributors to total flux, although their contributions varied with depth. Phytoplankton flux was more important from the upper to lower EZ; fecal pellets were more important at the EZ base and below. C:N elemental ratios and ^{13}C and ^{15}N isotope analyses indicated particle transformations within and beneath the EZ. ^{234}Th-^{238}U disequilibrium measurements varied, likely reflecting the mixing of water from multiple regions over the ~month-long time-scale of ^{234}Th. Our results highlight the complexity of the biological carbon pump in oligotrophic regions.

KEYWORDS: biological carbon pump; sinking particles; mesopelagic flux attenuation; phytoplankton; ^{238}Uranium-^{234}Thorium disequilibrium

available online at academic.oup.com/plankt

© The Author(s) 2021. Published by Oxford University Press. All rights reserved. For permissions, please e-mail: journals.permission@oup.com.

Downloaded from https://academic.oup.com/plankt/advance-article/doi/10.1093/plankt/fbab001/6129944 by Florida State University Law Library user on 08 February 2021

INTRODUCTION

Photosynthesis in the euphotic zone (EZ) removes CO_2 from the surface ocean, reducing the partial pressure of CO_2 and leading to CO_2 flux from the atmosphere into the ocean. However, because phytoplankton have very short life spans, long-term carbon sequestration requires transport of organic carbon into the deep ocean via processes collectively referred to as the biological carbon pump (BCP) (Volk and Hoffert, 1985; Ducklow *et al.*, 2001; Siegel *et al.*, 2016; Boyd *et al.*, 2019). These transport processes include active transport mediated by diel vertical migrants (Steinberg *et al.*, 2000; Archibald *et al.*, 2019), passive transport of refractory dissolved organic matter (Carlson *et al.*, 1994; Hansell *et al.*, 2009), and subduction and mixing of particles to depth (Omand *et al.*, 2015; Stukel *et al.*, 2018). However, in most of the ocean, the dominant process in carbon flux to depth is believed to be gravitational sinking of a diverse suite of particles including phytodetritus, fecal pellets, and aggregates of mixed origin (Turner, 2015). Estimates of the BCP's global magnitude range from 5–12 Pg C yr^{-1}, highlighting both its importance to the global carbon cycle and the substantial uncertainty in our understanding of the BCP (Henson *et al.*, 2011; Laws *et al.*, 2011; Siegel *et al.*, 2014).

In the vast oligotrophic regions of the world ocean, much of our understanding of the BCP comes from time-series studies in the Sargasso Sea and North Pacific Subtropical Gyre (Church *et al.*, 2013; Lomas *et al.*, 2013). These studies generally depict an inefficient BCP in low-productivity regions with only ~5% of net primary production (NPP) exiting the EZ. However, substantial spatial and temporal variability exists at multiple scales, suggesting variability in the dynamics driving the BCP in these regions (Estapa *et al.*, 2015; Laws and Maiti, 2019). In more spatially heterogeneous regions, inverse correlations between export efficiency and NPP have also called into question the assumption that oligotrophic regions have uniformly low export efficiencies (Maiti *et al.*, 2013; Kelly *et al.*, 2018; Kahru *et al.*, 2019).

The open-ocean Gulf of Mexico (GoM) is an interesting oligotrophic study site with similarities and important contrasts to the Sargasso Sea (Bermuda Atlantic Time Series, BATS) and North Pacific Subtropical Gyre (Hawaii Ocean Time-series, HOT). The GoM has similarly low NPP, low nutrients, and deep chlorophyll maxima (DCM) (Biggs, 1992; Gomez *et al.*, 2018; Shropshire *et al.*, 2020; Yingling *et al.*, this issue). However, it is also a mostly enclosed basin with strong coastal-offshore lateral gradients and very high mesoscale activity driven in part by the Loop Current and the eddies it sheds (Oey *et al.*, 2005; Zhong and Bracco, 2013; Green *et al.*, 2014). Prior studies of the BCP in the GoM using sediment traps and ^{234}Th have suggested a system with low to moderate export efficiency. Hung *et al.* (2004) found substantial differences in POC flux on two GoM cruises with carbon export ranging from 5.0–12.3 mmol C m^{-2} d^{-1} on a cruise in July 2000 and only 3.1–3.8 mmol C m^{-2} d^{-1} the following May, although, on both cruises, flux was higher beneath cold-core rings than beneath warm-core rings. In two subsequent cruises, however, warm-core rings occasionally had higher export than cold-core rings (Hung *et al.*, 2010). Taken together, these studies suggest higher export efficiency than found at BATS or HOT, with average *e*-ratios (export/NPP) of 0.13 in warm core rings and 0.18 in cold-core rings. Maiti et al. (2016), however, sampled a broadly similar area in March of 2012 and 2013 (a more productive season in the GoM) and found an average *e*-ratio of 0.07, which is much more similar to HOT than BATS.

In the open-ocean GoM, sinking particles may play important roles in the ecosystem beyond carbon sequestration. After the Deepwater Horizon oil spill, flocculation and sinking of oil-associated marine snow was an important removal term for water column hydrocarbons (Daly *et al.* 2016; Passow *et al.*, 2012; Passow, 2016). Carbon export also supports benthic communities, including commercially important fish, while contributing to the spread of hypoxic zones in the northern GoM (Biggs *et al.*, 2008). Sinking particles within the EZ may serve as important connections between different layers of this highly stratified environment. Many commercially important fish live in discrete depth horizons within the EZ during their vulnerable pelagic larval stages (Rooker *et al.*, 2012; Habtes *et al.*, 2014; Cornic *et al.*, 2018). Exceedingly deep, light-limited DCM (often > 100 m deep) in the GoM and other open-ocean regions are inhabited by distinct flora and fauna from the surface mixed layer and respond to different biogeochemical forcing. In regions with low vertical velocity and weak eddy diffusivity, sinking particles and vertically migrating taxa may be the main mechanisms linking upper and lower EZ communities.

Our goal in this study is to investigate particle flux within and beneath the EZ in highly stratified, oligotrophic regions of the GoM. This study is embedded within a larger whole-ecosystem project (Bluefin Larvae in Oligotrophic Ocean Foodwebs: Investigating Nutrients to Zooplankton in the Gulf of Mexico, BLOOFINZ-GoM) that provides substantial context about local biogeochemistry and plankton communities (Gerard *et al.*, this issue). Quantification of flux and characterization of sinking particles within the EZ and mesopelagic allows us to identify net particle production regions and assess transformations occurring as organic matter sinks through the water column.

Downloaded from https://academic.oup.com/plankt/advance-article/doi/10.1093/plankt/fbab001/6129944 by Florida State University Law Library user on 08 February 2021

Table I: Cycle overview data. Deployment date (m/d/y), recovery date (m/d/y), deployment latitude (Lat, °N) and longitude (Lon, °W), EZ depth (Euph, 0.1% surface irradiance, m), mixed layer depth (MLD, Δ0.1 kg m^{-3} from 10 m depth), deep chlorophyll maximum depth (DCM, m) and surface Chl a (Chl a, μg L^{-1})

Cycle	Deploy	Recover	Lat	Lon	Euph	MLD	DCM	Chl *a*
1	5/10/17	5/14/17	26.12	87.78	134	30	99	0.10
2	5/16/17	5/18/17	25.99	89.25	139	24	120	0.08
3	5/27/17	5/30/17	26.64	90.20	150	28	137	0.07
4	5/05/18	5/08/18	27.33	89.51	133	24	109	0.10
5	5/14/18	5/19/18	28.36	87.22	128	12	78	0.12

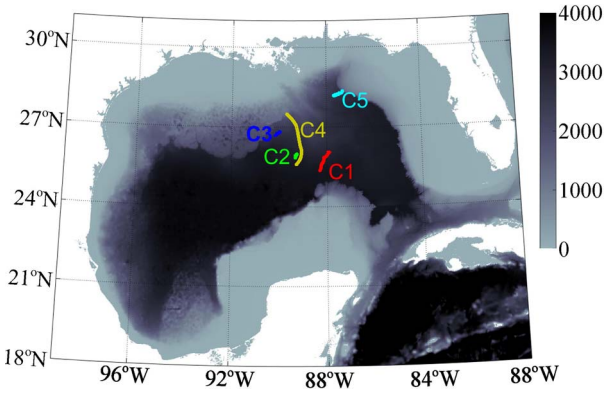

Fig. 1. Map of study site showing bathymetry (m) and Lagrangian cycle drift tracks.

METHODS

Experimental design

The BLOOFINZ-GoM cruises in April–May 2017 and May 2018 were designed to investigate the biogeochemistry and food web ecology of the open-ocean ecosystems where Atlantic bluefin tuna spawn (Fig. 1). We used a sampling scheme centered around 2–5 day duration Lagrangian experiments (hereafter 'cycles', referred to as C1—C5, Table I). At the beginning of each experiment, we deployed a sediment trap array (details below). We also deployed an *in situ* incubation array for 24 h during each day of every cycle, to which we attached experimental bottles used to measure primary productivity, protistan grazing rates, and phytoplankton growth rates (Landry *et al.*, this issue; Yingling *et al.*, this issue). Both arrays included a satellite-enabled surface float and a 3 × 1-m holey sock drogue centered at 15-m depth to ensure that the Lagrangian arrays traveled with the surface mixed layer (Landry *et al.*, 2009; Stukel *et al.*, 2015). We also conducted day-night CTD-Niskin rosette casts and zooplankton net tows near the drifter locations to collect samples for particulate organic matter, nutrients, chlorophyll *a*, phaeopigments, ^{234}Th activity, and mesozooplankton biomass each day of the cycle (Knapp *et al.*, this issue; Landry and Swalethorp, this issue).

^{238}U-^{234}Th disequilibrium

We measured ^{234}Th activity using a standard small-volume protocol (Benitez-Nelson *et al.*, 2001b; Pike *et al.*, 2005). Samples (2–4 L) were collected from Niskin bottles and immediately acidified with HNO_3^- to a pH < 2 and spiked with ^{230}Th yield tracer. The bottles were vigorously shaken and allowed to equilibrate for 4–9 hours. We then re-basified the sample with NH_4OH to a pH of 8–9 and added $MnCl_2$ and $KMnO_4$. Samples were again shaken and allowed to equilibrate for >8 h before vacuum filtering at high pressure through a quartz (QMA) filter to collect manganese oxide precipitate. Post-cruise samples were counted on two RISO low-background beta multi-counters multiple times during the decay process of ^{234}Th. After background counting (>6 half-lives after collection), samples were dissolved in H_2O_2/HNO_3^- solution, and ^{229}Th was added as a second yield tracer. Thorium was then purified by column chromatography using AG1-X8 resin. $^{229:230}$Th ratios were measured using inductively coupled plasma mass spectrometry at the National High Magnetic Field Laboratory. $^{229:230}$Th ratios were used to determine the initial yield of thorium filtration.

Because the water column was very stable, as determined by Thorpe-scale analysis (Gargett and Garner, 2008; Kelly *et al.*, in review), and environmental conditions in the region remained relatively constant throughout the cycles, we used a simple one-dimensional steady-state equation to compute ^{234}Th export (E_{234Th}, units of dpm m^{-2} d^{-1}):

$$E_{234Th} = \lambda_{234}\,(A_{238U} - A_{234Th})$$

where λ_{234} is the decay constant for ^{234}Th (d^{-1}), A_{238U} is the vertically integrated activity of ^{238}U (dpm m^{-3}), and A_{234Th} is the vertically integrated activity of ^{234}Th (dpm m^{-3}) (Savoye *et al.*, 2006). ^{238}U activity was estimated from salinity following Owens *et al.* (2011). We note,

Downloaded from https://academic.oup.com/plankt/advance-article/doi/10.1093/plankt/fbab001/6129944 by Florida State University Law Library user on 08 February 2021

however, that this equation neglects lateral advection, which may be important in regions, like the GoM, with strong spatial gradients. To determine carbon export from thorium export, we multiplied by the C:^{234}Th ratio of sediment trap-collected particles (see below). Between sediment trap sampling depths, we linearly interpolated C:^{234}Th measurements.

Sediment traps

We deployed VERTEX-style, surface-tethered drifting sediment traps (Knauer *et al.*, 1979). The trap array included surface floats, a 3 × 1-m holey-sock drogue centered at 15-m that ensured that our array followed the mixed layer while also dampening vertical displacement caused by waves, and sediment trap cross-pieces at 3 depths. The shallowest depth of 60 m was within the EZ (beneath the mixed layer, but substantially above the deep chlorophyll maximum) and hence captured flux from the surface mixed layer to the deep EZ. The second cross-piece was placed at a variable depth chosen to be slightly below the depth of the EZ. This trap depth ranged from 117 to 151 m. The third cross-piece was consistently located at 231 m in the mesopelagic zone. Each cross-piece held 6–8 particle interceptor tubes, consisting of an acrylic tube (7-cm inner diameter, 8:1 aspect ratio) topped with a baffle consisting of 13 smaller, beveled acrylic tubes with similar 8:1 aspect ratios. Although sediment traps can be subject at times to hydrodynamic biases (Baker *et al.*, 1988; Buesseler *et al.*, 2007), extensive comparisons of flux results from the VERTEX-style array used in this study to contemporaneous ^{238}U-^{234}Th deficiency measurements have suggested no substantial over- or under-collection bias (Stukel *et al.*, 2019a). Baker et al. (2020) also recently found that surface-tethered VERTEX-style traps closely matched the results of cylindrical-shaped neutrally buoyant sediment traps (although conical traps appeared to under-collect sinking particles).

Tubes were deployed with a preserved brine composed of 0.1-μm filtered seawater amended with 50 g L^{-1} NaCl and 0.4% formaldehyde (final concentration). Deployment durations ranged from 2.2 to 4.5 days. After recovery, we identified the interface between overlying seawater and the formaldehyde brine and removed the overlying seawater by gentle suction. Samples were then filtered through a 100-μm Nitex filter. These filters were then inspected at 25X magnification under a stereomicroscope, and metazoan 'swimmers' were removed from the sample. The non-swimmer portion remaining on the 100-μm filter was then rinsed back into the sediment trap sample. Three tubes per depth were filtered through precombusted GF/F filters for particulate organic carbon (POC), particulate nitrogen, and stable isotope analysis. An additional tube's worth of formaldehyde brine was kept in a dark bottle for the duration of the deployment and similarly filtered to serve as a blank. GF/F filters were frozen at −80°C for the remainder of the cruise. Post-cruise, they were acidified with fuming HCl to remove inorganic carbon, then dried at 40°C and analyzed by an elemental analyzer interfaced with an isotope ratio mass spectrometer (IRMS) at the UC Davis Stable Isotope Facility. An additional three tubes were used for pigment and ^{234}Th analyses. The volumes of these tubes were measured, then the tubes were vigorously mixed and a 50 mL subsample (∼3% of the recovered sample volume) was filtered through GF/F filters for pigment analyses. These samples were immediately placed in a test tube with 7 mL acetone to extract for 24 h at −20°C. They were then analyzed for chlorophyll *a* and its degradation products (phaeopigments) using the acidification method (Strickland and Parsons, 1972). Pigments were not analyzed on C3. The remainder of the sample (∼97%) was filtered through a pre-combusted QMA filter for ^{234}Th analyses. These samples were analyzed using a beta multi-counter as described above.

To extrapolate flux between depths (necessary to quantify flux at exactly the base of the EZ), we fit a simple power law relationship to flux estimated from the sediment traps directly above and below the EZ. Results of this calculation were fairly insensitive to the extrapolation method chosen, because the second sediment trap depth was typically only ∼10 m from the depth of the EZ. For one cycle, we also extrapolated export flux to a depth 20 m beneath the deepest trap, by extending the power law relationship from the bottom two traps. When computing mean ratios of properties measured from the same tubes (e.g. chlorophyll:phaeopigments or carbon:nitrogen), we take the arithmetic mean of the ratios in replicate tubes and report standard error of the mean as the uncertainty. When computing mean ratios for properties measured in different tubes (e.g. carbon:chlorophyll), we take the ratio of the means and propagate the uncertainty from standard errors of the means.

Water column and plankton community measurements

Samples for water column POC, pigments, nutrients, and phytoplankton biomass were taken at 6 depths spanning the EZ from daily 02:00 CTD casts. 250-mL samples for chlorophyll *a* and phaeopigments were analyzed by the acidification method as described above (Landry *et al.*, this issue). Samples (2.2-L) were used for POC and analyzed as previously described. Nutrient concentrations ($NO_3^- + NO_2^-$) were measured using a chemiluminescent method (Knapp *et al.*, this issue). Phytoplankton

Downloaded from https://academic.oup.com/plankt/advance-article/doi/10.1093/plankt/fbab001/6129944 by Florida State University Law Library user on 08 February 2021

biomass was determined from a combination of flow cytometry and epifluorescence microscopy (Selph *et al.*, this issue). Briefly, samples for microscopy were preserved, stained with DAPI (nucleic acid stain) and proflavin (protein stain), then filtered through 0.8-μm (nanoplankton) or 8.0-μm (microplankton) black polycarbonate filters. Cells were analyzed using image analysis (Taylor *et al.*, 2015). DAPI fluorescence was used to identify living cells, while proflavin fluorescence showed cell outlines for morphometric measurements (length, width, area) to estimate biovolume. Phototrophic status was determined from chlorophyll autofluorescence. Cellular carbon was determined from biovolume and carbon:volume conversion factors (Menden-Deuer and Lessard, 2000). Picophytoplankton (*Prochlorococcus*, *Synechococcus* and picoeukaryotes) abundances were determined from flow cytometry (Selph *et al.*, 2011). Cells enumerated from microscopy in the 2–5 μm size range were subtracted from flow cytometry-derived eukaryote abundance to exclude nanoeukaryotes from our picoeukaryote abundance estimates. Picophytoplankton biomass was estimated from cell abundance by multiplying by literature-based cellular carbon conversions. For additional details, see Selph *et al.* (this issue) and Landry *et al.* (this issue). Summed carbon biomass measurements were used to determine the C:Chl ratio of phytoplankton communities as a function of depth. We computed C:Chl ratios as the ratio of total phytoplankton biomass to acidification-method determined Chl *a*, to be consistent with acidification-method determined C:Chl ratios in sediment traps. We note, however, that Selph *et al.* (this issue) provides C:Chl ratios based on the more accurate HPLC method (not available for sediment trap samples). Heterotrophic plankton biomass was determined as the sum of heterotrophic bacteria biomass (flow cytometry, Selph *et al.*, 2011) and nano- and microzooplankton biomass. Nano- and microzooplankton biomass was determined from the sum of the non-pigmented cells (epifluorescence microscopy, described above) and ciliate biomass determined from inverted light microscopy of acid Lugol's preserved samples (Landry *et al.*, this issue). Living POC was defined as the sum of the carbon biomass of phytoplankton and heterotrophic plankton (bacteria + protists). NPP was measured by $H^{13}CO_3^-$ uptake (Yingling *et al.*, this issue). Briefly, triplicate 2.8-L polycarbonate bottles and an additional 'dark' polycarbonate bottle were gently filled from Niskin bottles. Samples were spiked with ^{13}C-labeled HCO_3^- and incubated *in situ* on our incubation array at the depths from which they were sampled to ensure natural light and temperature conditions. After 24 hours, samples were recovered, filtered, and the incorporation of ^{13}C into phytoplankton biomass was determined by IRMS. Mesozooplankton grazing rates were determined from gut pigment measurements made on samples derived from paired day-night oblique bongo net tows (surface to 100-m depth on NF17 and surface to ∼135 m on NF18, 200-μm mesh, Landry and Swalethorp, this issue). Additional details for all plankton community measurements are available in the previously cited manuscripts.

RESULTS

Ecosystem structure during Lagrangian experiments

During April–May 2017 and May 2018, our study region was characterized by very deep DCM. Cycle-average mixed-layer chlorophyll *a* ranged from 0.07 (C3) to 0.12 (C5) μg L^{-1}. Cycle-average DCM depth varied from 80 m on C5 to 140 m on C3 (Fig. 2a). DCM-average chlorophyll *a* ranged from 0.26 (C3) to 0.81 (C5) μg L^{-1}. DCM were also phytoplankton biomass maxima on C1 and C5 (Fig. 2d). On C4, there was no significant deep biomass maximum found, and the DCM primarily reflected photoadaptation processes as phytoplankton in the deep water column exhibited decreased carbon:chlorophyll ratios relative to mixed-layer communities (phytoplankton biomass was not quantified on C2 or C3). The C:Chl ratio varied from ∼50–120 (g:g) in the upper EZ to 10–36 at the DCM. The DCM depth was typically near the 1% incident light level, which varied from 86 to 112 m. The 0.1% incident light level varied from 128 to 150 m depth and was used as the depth of the EZ in future calculations. The mixed layer depth was consistently shallow (defined as a difference of 0.1 kg m^{-3} relative to the density at 10 m) and ranged from 12 to 32 m.

POC concentrations showed low variability with depth or between cycles; cycle-average concentrations were between 4 and 8 mmol C m^{-3} at almost all EZ depths. Only C1 and C4 had higher POC concentrations (8–10 mmol C m^{-3} near the surface). The lowest measured POC was found at depths of 90 and 100 m on C5. As this was the cycle with the shallowest DCM and EZ, these samples were actually from beneath the EZ. The proportion of this POC that was contained in live organisms (bacteria, phytoplankton, and non-pigmented protists) was lower in the mixed layer (∼20%) than near the DCM (20–60%, Fig. 2c).

Despite the strong DCM and typically increasing phytoplankton biomass with depth, NPP declined substantially and nearly monotonically with depth (Fig. 2f). Cycle-average surface NPP varied from 0.27 to 0.55 mmol C m^{-3} d^{-1}, while NPP at the DCM was

Downloaded from https://academic.oup.com/plankt/advance-article/doi/10.1093/plankt/fbab001/6129944 by Florida State University Law Library user on 08 February 2021

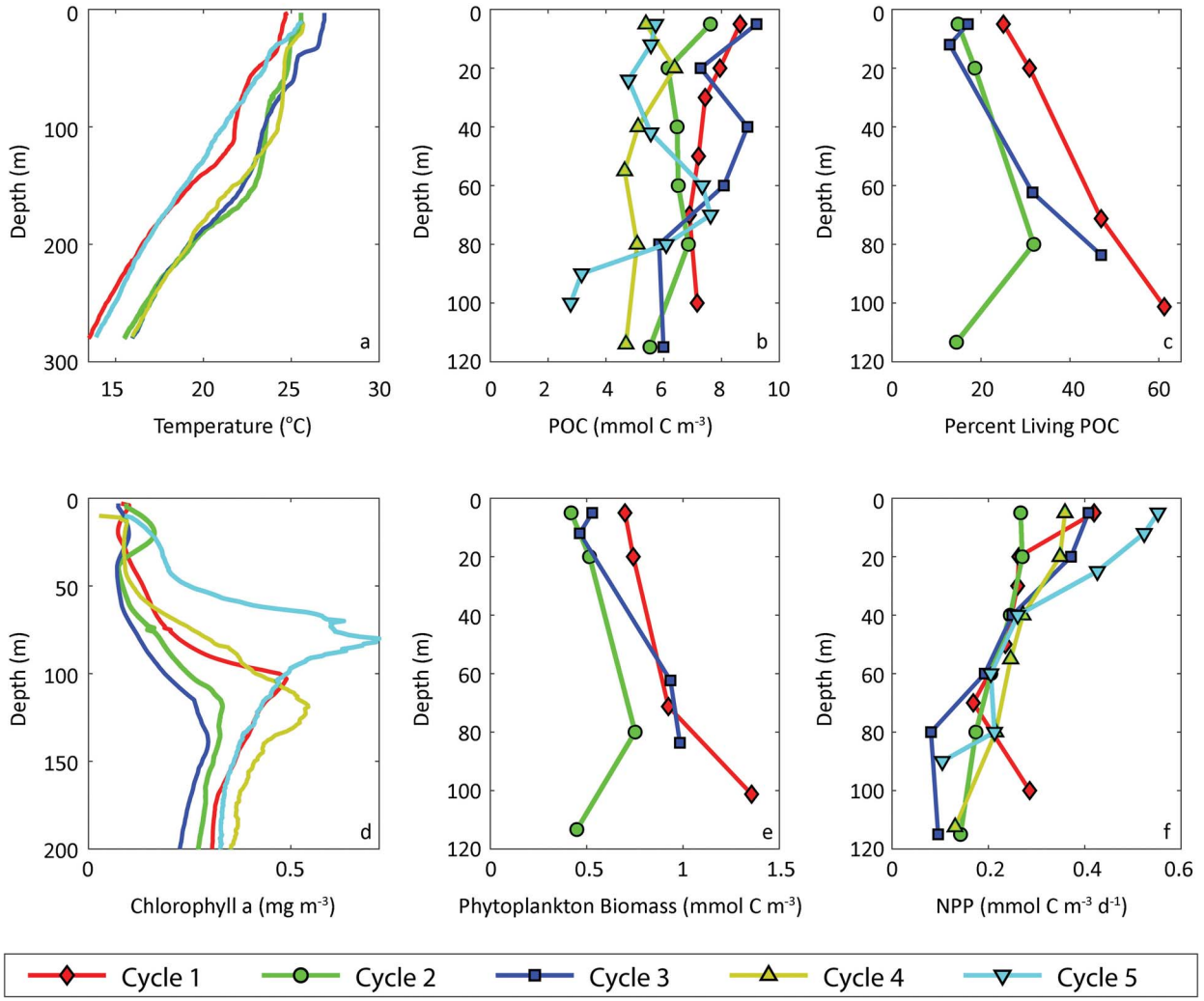

Fig. 2. Cycle-average vertical profiles: Temperature (**a**). Particulate organic carbon (**b**). Percentage of POC contained in living biomass, defined as heterotrophic bacteria + cyanobacteria + autotrophic protists + non-pigmented protists (**c**). Chlorophyll (**d**). Chlorophyll profiles are interpolated between and beneath sampling points using CTD fluorescence profiles. Phytoplankton biomass (**e**). NPP (**f**).

< 0.14 for all cycles except C1. On this 3-day cycle, two NPP daily profiles gave a monotonic decrease of NPP with depth (within the accuracy of the measurement), but the third profile showed a monotonic decrease from the surface to 70 m, followed by a substantial increase in NPP at the DCM, where autotrophic eukaryote biomass was high. Although surface NPP varied by a factor of ∼2 between cycles, vertically integrated NPP was relatively invariant among cycles (24.9–29.3 mmol C m^{-2} d^{-1}), because cycles with high surface NPP also had shallower EZs. Across the 5 cycles, 62 to 79% of measured NPP occurred at a depth shallower than 60 m (the depth of our shallow sediment trap), while 21 to 38% occurred between 60 m and the DCM. There was also likely some additional production beneath our deepest sampling depth, although we believe that NPP would have declined rapidly beneath the DCM because phytoplankton biomass declined rapidly and specific rates (strongly correlated with photosynthetically active radiation in the deep EZ) would also have declined.

Sediment trap–derived sinking flux estimates

POC flux quantified using sediment traps ranged from 3.6 to 8.9 mmol C m^{-2} d^{-1} at 60 m. Carbon flux declined between this mid-euphotic zone trap and the trap at the base of the EZ on 4 of the 5 cycles (Fig. 3; Table II). During the other cycle (C3), flux increased from 6.6 ± 1.0 mmol C m^{-2} d^{-1} at 60 m to 6.9 ± 0.4 mmol

Downloaded from https://academic.oup.com/plankt/advance-article/doi/10.1093/plankt/fbab001/6129944 by Florida State University Law Library user on 08 February 2021

Table II: Sediment trap-derived export flux in each cycle. Organic carbon (Carbon, mmol C m^{-2} d^{-1}), nitrogen (Nitrogen, mmol N m^{-2} d^{-1}), chlorophyll (Chl a, μg m^{-2} d^{-1}), phaeopigments (Phaeo, μg Chl a equiv. m^{-2} d^{-1}), ^{234}Th (dpm m^{-2} d^{-1}) and isotopic composition of carbon ($\delta^{13}C$) and nitrogen ($\delta^{15}N$).

Cycle	Depth	Carbon	Nitrogen	Chl *a*	Phaeo	^{234}Th	δ^{13}C	δ^{15}N	NPP	EZ	T_{100}
1	60	8.9 ± 1	1.5 ± 0.3	17 ± 5	23 ± 12	477 ± 39	−22.2 ± 0.1	2.9 ± 0.1			
	140	3.4 ± 0.1	0.5 ± 0	14 ± 3	94 ± 12	697 ± 48	−23.8 ± 0.0	4.9 ± 0.2	25.6 ± 1.3	0.138	0.657
	231	2.3 ± 0.5	0.2 ± 0	1 ± 2	65 ± 20	983 ± 66	−25.2 ± 0.8	4.2 ± 0.1			
2	60	6 ± 0.2	0.8 ± 0	16 ± 3	4 ± 2	668 ± 45	−22.3 ± 0.2	2.5 ± 0.3			
	140	3.7 ± 0.7	0.5 ± 0.1	44 ± 5	64 ± 22	813 ± 38	−23.6 ± 0.4	2.9 ± 0.1	24.3 ± 1.5	0.154	0.578
	231	2.3 ± 0.1	0.2 ± 0	38 ± 37	77 ± 12	895 ± 17	−23.8 ± 0.5	3.5 ± 0.2			
3	60	6.6 ± 1.1	1 ± 0.1	n.d.	n.d.	474 ± 62	−21.7 ± 0.1	1.7 ± 0.1			
	140	6.9 ± 0.4	1.1 ± 0.1	n.d.	n.d.	803 ± 60	−22.7 ± 0.4	3.7 ± 0.9	24.9 ± 2.2	0.248	0.437
	231	3.1 ± 0.4	0.4 ± 0.1	n.d.	n.d.	798 ± 29	−23.4 ± 0.2	3.7 ± 0.1			
4	60	3.6 ± 0.1	0.6 ± 0	7 ± 1	5 ± 1	546 ± 22	−22.4 ± 0.0	2.5 ± 0.1			
	151	3.1 ± 0.4	0.5 ± 0.1	17 ± 12	157 ± 65	1 059 ± 32	−23.4 ± 0.2	3.7 ± 0.2	28.6 ± 1.1	0.111	0.525
	231	1.7 ± 0	0.2 ± 0	74 ± 73	118 ± 3	1 113 ± 20	−23.9 ± 0.1	4.7 ± 0.1			
5	60	7.2 ± 0.3	1.1 ± 0	31 ± 3	23 ± 8	475 ± 26	−22.4 ± 0.0?	3.8 ± 0.1			
	117	5.8 ± 0.6	0.9 ± 0.1	52 ± 14	283 ± 86	832 ± 24	−23.4 ± 0.1	4.6 ± 0.1	29.3 ± 1.3	0.178	0.486
	231	2.5 ± 0.2	0.3 ± 0	−1 ± 2	125 ± 22	1 128 ± 99	−23.6 ± 0.1	5.0 ± 0.1			

Last three columns give NPP (mmol C m^{-2} d^{-1}), export efficiency at the base of the EZ and transfer efficiency through the upper 100 m of the twilight zone (T_{100}). Uncertainties are the standard error of the mean.

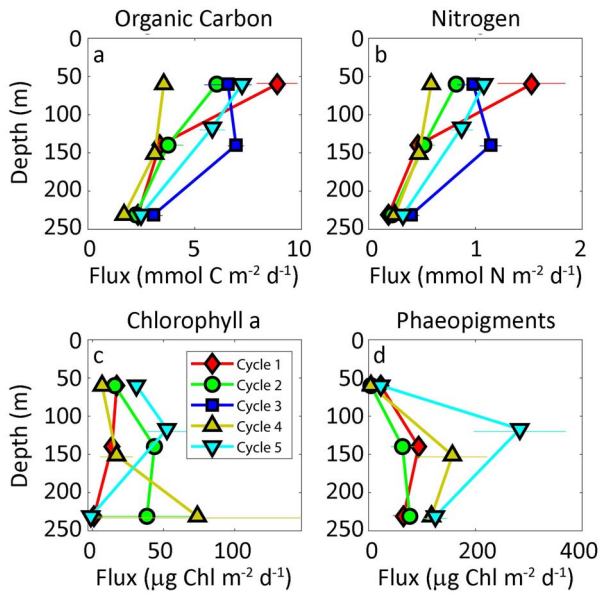

Fig. 3. Vertical flux of sinking POC (**a**), particulate nitrogen (**b**), chlorophyll *a* (**c**), and phaeopigments measured in sediment traps. Error bars are standard error of the mean.

C m^{-2} d^{-1} at 140 m, although fluxes measured at these depths were not statistically different. The greatest decline in flux occurred on C1, decreasing by 62% between 60 and 140 m. This flux decline within the deep EZ occurred despite the fact that approximately one-third of NPP occurred in this depth stratum. Particulate nitrogen flux similarly declined with depth through the EZ. Unsurprisingly, flux declined further beneath the EZ. At 231 m, POC flux ranged from 1.7 to 3.1 mmol C m^{-2} d^{-1}.

C:N ratios of sinking particles were relatively constant within the EZ (shallow trap and middle depth trap) and slightly more nitrogen rich than the standard Redfield ratio of 106:16 (mol:mol, Fig. 4a). The C:N ratio of sinking particles consistently increased from the base of the EZ to the mesopelagic trap at 231 m. Sometimes, the increase was negligible (e.g. 5.7 ± 0.03 to 5.9 ± 0.3 on C4); at other times, it was substantial (6.2 ± 0.08 to 10.6 ± 1.7 on C1). In contrast, the isotopic ratios of sinking material showed a greater shift between the shallow and middle traps than between the middle and deep traps. δ^{13}C typically declined by ∼ 1‰ from the middle of the EZ to the base of the EZ and by a lesser amount from the base of the EZ to the deep trap. δ^{15}N increased from an average of 2.7 in the middle of the EZ to 3.9 at the base of the EZ, with three cycles showing a further increase into the mesopelagic and two cycles showing a decrease beneath the EZ. These isotopic changes likely reflect a greater importance of recycled nitrogen in the upper EZ relative to the DCM and preferential remineralization of ^{14}N by attached microbial communities.

Pigment flux can be used to investigate the importance of direct phytoplankton sinking and fecal pellets of herbivorous zooplankton to carbon export. Chlorophyll flux in the middle of the EZ (60 m depth) ranged from 7 to

Downloaded from https://academic.oup.com/plankt/advance-article/doi/10.1093/plankt/fbab001/6129944 by Florida State University Law Library user on 08 February 2021

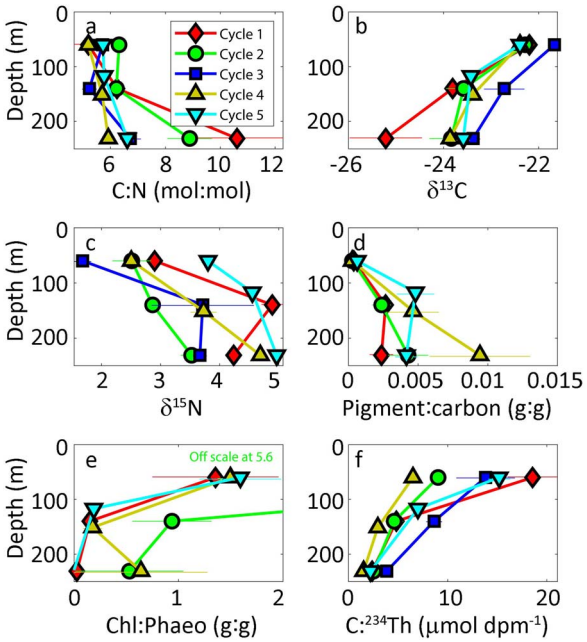

Fig. 4. Characterization of sinking particles collected in sediment traps: carbon:nitrogen ratio (**a**), $\delta^{13}C$ (**b**) $\delta^{15}N$ (**c**), total pigment:carbon ratio (total pigment = chlorophyll a + phaeopigments, (**d**), chlorophyll:phaeopigment ratio (**e**), and C:^{234}Th ratio. Note that one point in the chlorophyll:phaeopigments ratio graph is off scale with a value of 5.6 g:g at 60 m for cycle 2. Error bars are standard error of the mean.

31 μg Chl *a* m^{-2} d^{-1} (Fig. 3). This yielded C:Chl (g:g) ratios ranging from 2 802 to 6 274. These ratios were substantially greater than mixed-layer C:Chl ratios for living phytoplankton (~50 to 120 g:g), suggesting that intact phytoplankton comprised a very small fraction of sinking particulate matter. Pigment flux actually increased from the middle of the EZ to the base of the EZ, and the C:Chl ratio of sinking material declined to 1 032–2 944 at the base of the EZ, which might indicate a slightly higher proportion of sinking phytoplankton. However, at the DCM, the C:Chl ratio of intact phytoplankton declined to 10–36, due to cellular photoacclimation. Thus, whether phytoplankton were slightly more or slightly less important to flux at the base of the EZ depends on where those phytoplankton originated and whether or not they underwent photoacclimation as they sank. Chlorophyll flux declined beneath the EZ, except on C4, where very low chlorophyll was measured in two of the three replicate sediment trap tubes, but the third tube had chlorophyll concentrations equivalent to a flux of 220 μg Chl a m^{-2} d^{-1}.

The ratio of chlorophyll to phaeopigments (which are the degradation product of acidified chlorophyll *a* and typically produced as a byproduct of zooplankton grazing) can be used to assess the relative importance to sinking carbon of phytoplankton and the fecal pellets of herbivores. Chl:Phaeo ratios of sinking particles were greater than 1.0 at 60 m, suggesting that phytoplankton contributed more to flux out of the EZ than the fecal pellets of herbivores (Fig. 4e). However, at deeper depths, the Chl:Phaeo ratio of sinking particles decreased substantially, 6- to 8-fold lower at the base of the EZ than at 60 m. Both chlorophyll and phaeopigment fluxes typically decreased in the mesopelagic zone, although their ratio was variable at depth.

Export efficiency was moderate. The *e*-ratio (sediment trap carbon flux/NPP) assessed at the base of the EZ ranged from 11% (C4) to 25% (C3), with a cross-cycle mean of 16.6%. Notably, if the *e*-ratio was computed for the upper EZ only (i.e. export flux at 60 m/NPP above 60 m), it would have been much higher, ranging from 19 to 53%. This suggests that a higher proportion of produced particles sink from the upper EZ even if these particles do not sink far enough to exit the base of the EZ. Particle flux attenuation in the mesopelagic was also fairly moderate. T_{100} values (export flux at euphotic depth plus 100 m/export flux at euphotic depth) ranged from 44 to 66% indicating that slightly less than 50% of sinking carbon is remineralized, on average, in the first 100 m of the twilight zone.

Thorium-derived export flux estimates

^{238}U-^{234}Th showed remarkably low variability with depth, and in most profiles, ^{234}Th activity was only slightly less than ^{238}U activity (as predicted from salinity measurements, Fig. 5a–e). C5, with the shallowest DCM and also closest to the shelf break in the northeastern GoM, had the highest surface ^{238}U-^{234}Th deficiency (~0.8 dpm L^{-1}) and also the strongest vertical gradient, as deficiency decreased with depth. C2 exhibited net negative deficiency at most depths (i.e. ^{234}Th > ^{238}U) although at most depths ^{234}Th was not significantly different from equilibrium with ^{238}U. Excepting C2, for which a ^{234}Th export model predicted negative export, all cycles gave increasing ^{234}Th export with depth from the surface to at least 170 m. This agreed with sediment trap results, which showed monotonically increasing ^{234}Th flux with depth except for the two deepest traps of C3, for which ^{234}Th export was not statistically different (803 ± 60 versus 798 ± 29 dpm m^{-2} d^{-1} at 140 and 231 m, respectively). ^{234}Th export, as assessed by both sediment traps and the ^{238}U-^{234}Th deficiency model, was higher for the two NF1802 cycles than the three NF1704 cycle experiments.

To compute carbon export from ^{238}U-^{234}Th deficiency measurements, we multiplied predicted ^{234}Th export by the C:^{234}Th ratios of sinking particles collected in sediment traps (Fig. 4f). These ratios decreased

Downloaded from https://academic.oup.com/plankt/advance-article/doi/10.1093/plankt/fbab001/6129944 by Florida State University Law Library user on 08 February 2021

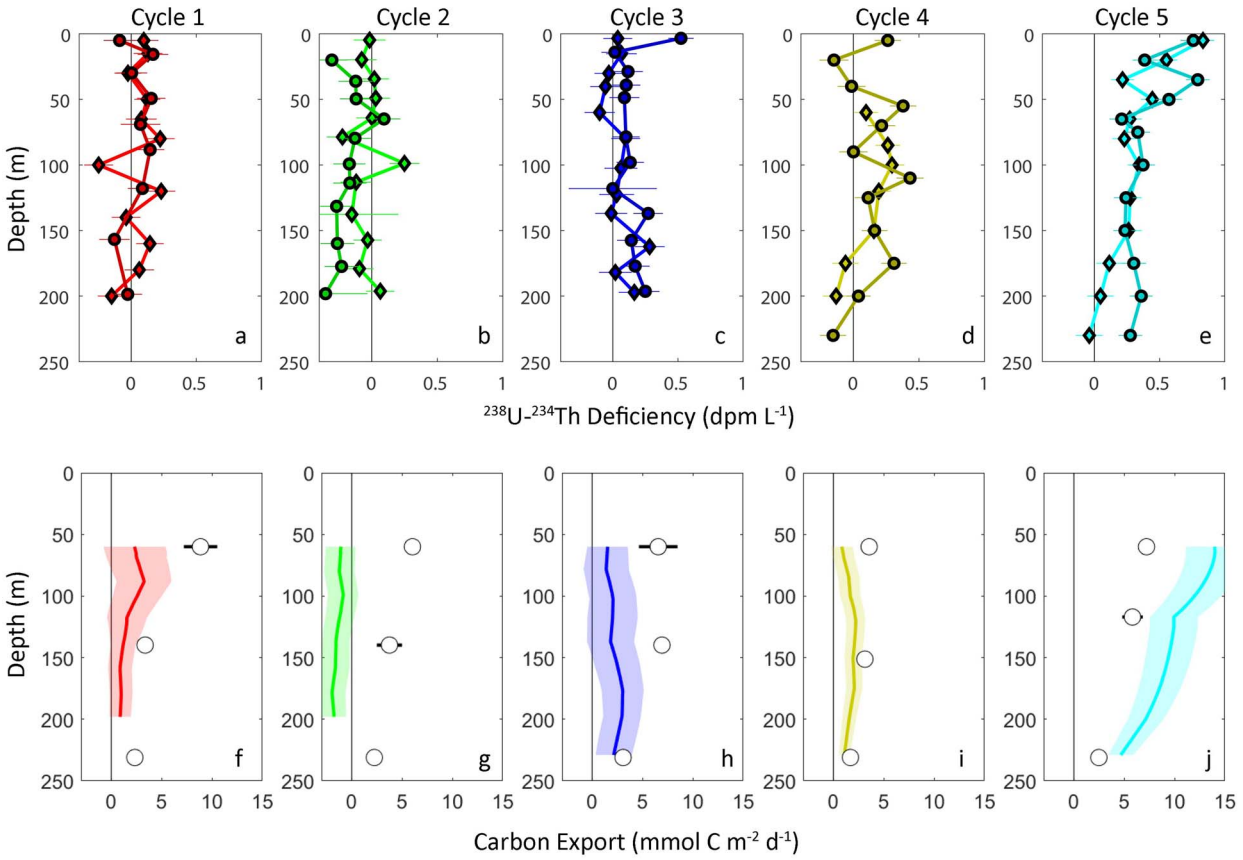

Fig. 5. ^{238}Uranium-^{234}Thorium deficiency (**a**-**e**) and carbon export computed from ^{238}U-^{234}Th deficiency (**f**-**j**). Open symbols in f-j are sediment trap-derived carbon export for the same cycles. Error bars are standard error of the mean.

substantially with depth. In the middle of the EZ (60 m), cycle-average C:^{234}Th ratios ranged from 6.5 to 18.6 μmol dpm^{-1} (median = 13.8 μmol dpm^{-1}). In the mesopelagic (231 m), the ratios varied from 1.5 to 3.9 μmol dpm^{-1} (median = 2.4 μmol dpm^{-1}). As a result of this strongly decreasing C:^{234}Th ratio with depth, vertical profiles of carbon export suggested midwater flux peaks that were typically within the EZ (Fig. 5f–j).

Overall, carbon export fluxes based on ^{238}U-^{234}Th deficiency showed much greater variability than carbon export fluxes measured directly by sediment traps. This result might seem surprising, since ^{234}Th integrates over a much longer period of time (~one month) than our sediment trap deployments (~4 days). However, it likely reflects the spatial variability and high mesoscale activity of the northern GoM. All of our sampling sites were in oligotrophic regions with low chlorophyll, low nutrients, and low plankton biomass, and the contemporaneous sediment trap deployments reflected these conditions. The ^{234}Th deficiency measurements integrate over the prior month, and as a result of relatively strong lateral gradients and high horizontal velocities along mesoscale features, they thus may reflect conditions on the shelf or in distinctly different oligotrophic regions (e.g. Loop Current). For these reasons, we consider the sediment trap results to reflect more accurately the carbon fluxes in the open-ocean study region.

DISCUSSION

Flux attenuation and vertical connectivity

The depth at which organic matter is remineralized largely determines how long the respired CO_2 will be sequestered from the atmosphere and hence has a large impact on atmospheric CO_2 concentrations (Kwon *et al.*, 2009). Flux attenuation is often modeled as a power law decrease from flux at a reference depth, usually taken to be the base of the EZ (Martin *et al.*, 1987). The exponents of such power laws have been shown to be highly variable (Marsay *et al.*, 2015), reflecting variability in particle sinking rates and multiple different

Downloaded from https://academic.oup.com/plankt/advance-article/doi/10.1093/plankt/fbab001/6129944 by Florida State University Law Library user on 08 February 2021

mechanisms within the mesopelagic that drive particle consumption or remineralization (Steinberg *et al.*, 2008; Trull *et al.*, 2008; McDonnell and Buesseler, 2010; Belcher *et al.*, 2016; Stukel *et al.*, 2019b). Alternate formulations have also been suggested to model different shapes of particle flux attenuation in the mesopelagic (Armstrong *et al.*, 2002; Buesseler and Boyd, 2009). Fundamentally, however, these views of the biological pump permit carbon sequestration processes to be split into two different parameters: export efficiency from the base of the EZ (i.e. EZ-ratio = *e*-ratio evaluated at base of EZ) and transfer efficiency through the mesopelagic (e.g. T_{100} = sinking flux at a depth 100 m deeper than the EZ divided by sinking flux at the base of the EZ) (Buesseler and Boyd, 2009).

Our results show, however, that net particle remineralization can begin within the middle of the EZ. Mean flux at 60 m was 6.4 mmol C m^{-2} d^{-1}. Mean flux at the base of the EZ (128–150 m) was 4.4 mmol C m^{-2} d^{-1}, indicating that 32% of sinking carbon, on average, was remineralized in the deep EZ (i.e. the depth strata encompassing the DCM). This net remineralization within the deep EZ occurred despite NPP rates that ranged from 6.1 to 10.3 mmol C m^{-2} d^{-1}. Although few studies have reported sediment trap–derived export flux in the middle of the EZ, Hung *et al.* (2010) also deployed euphotic-zone traps in the GoM. They found higher export flux at 65 m than at 120 m (base of EZ) on 4 out of 5 deployments, with an average flux of 6.9 mmol C m^{-2} d^{-1} at 65 m and an average flux of 5.2 mmol C m^{-2} d^{-1} at 120 m. Notably, our results also show that attempts to define zones of net particle remineralization from ^{234}Th profiles (e.g. Buesseler *et al.*, 2008a) can miss these shallow remineralization layers. In our study, both sediment traps and ^{238}U-^{234}Th deficiency profiles showed that ^{234}Th flux increased with depth in the water column. However, the decrease in C:^{234}Th ratios with depth was greater than the increase in ^{234}Th flux. Thus POC flux decreased even as ^{234}Th flux increased.

Net flux remineralization within the deep EZ suggests that sinking particles actually supply organic matter to the DCM. The DCM is thus not a layer of particle production, but rather a layer of net particle consumption and flux attenuation. Indeed, although NPP and phytoplankton growth rates declined at the DCM relative to the mixed layer, heterotrophic bacterial growth rates at the DCM were relatively similar to those above, with only slight decreases that are likely linked to temperature (Landry *et al.*, this issue). This suggests that bacterial production in the deep EZ relies, in part, on a subsidy of organic matter from above.

Although carbon and nitrogen mass fluxes decreased fairly consistently with depth, these results do not necessarily indicate that particles produced in the upper EZ exit through the base of the EZ. Rather, our results show distinct and replicable changes in particle characteristics with depth, some showing monotonic changes while others have more complicated patterns. For instance, C:^{234}Th and δ^{13}C decrease monotonically with depth, but C:N ratios of sinking particles are relatively constant within the EZ and increase in the mesopelagic. The C:^{234}Th patterns not only could reflect particle destruction and formation at multiple depths but also might be explained by continuing thorium sorption as slowly-sinking particles equilibrate with ambient ^{234}Th levels. Similarly, decreasing δ^{13}C with depth may represent particle turnover combined with generally declining δ^{13}C of DIC with depth through the epipelagic. Notably, however, the δ^{13}C of sinking particles collected in the deep GoM (1160–1660 m) was closer to our upper euphotic zone values than those measured at 231 m (Chanton *et al.*, 2018). The fairly constant C:N ratios of sinking particles at 60 m and at the base of the EZ, which are notably similar to typical Redfield C:N ratios for phytoplankton, seem to suggest that sinking material within and immediately beneath the EZ is similar to that of fresh phytoplankton. The higher C:N ratio of sinking particles in the mesopelagic likely reflects preferential N remineralization in the deep ocean.

Pigment:carbon ratios can be particularly useful for diagnosing the changing nature of sinking particles. The ratios at 60 m were quite low (mean = 0.0004 g:g), with chlorophyll *a* flux exceeding phaeopigment flux. If we assume that fresh sinking phytoplankton had Chl:C ratios representative of phytoplankton in the mixed layer (0.013 g:g), measured chlorophyll flux would indicate sinking phytoplankton fluxes of 0.11 mmol C m^{-2} d^{-1}, equivalent to < 2% of total sinking carbon. At the base of the EZ, pigment:carbon ratios increased by an order of magnitude (0.004 g:g), with pigment flux dominated by phaeopigments (5:1 Phaeo:Chl ratio). Considering that Chl:C ratios of phytoplankton at the DCM were 3.4-fold higher than in the mixed layer (compared to Chl:C ratios of sinking particles that were 2.8-fold higher beneath the chlorophyll max than beneath the upper EZ), this suggests a fairly comparable amount of sinking phytoplankton from the base of the EZ (relative to the upper EZ), but a substantial increase in the flux of fecal pellets derived from herbivory, the source of phaeopigments. This may reflect a prevalence of larger herbivores near the DCM, which had higher biomass of autotrophic eukaryotes than *Prochlorococcus*, and further emphasizes the biogeochemical impact of vertical structure within the EZ. The flux of herbivore fecal pellets diagnosed from pigments certainly underestimates total fecal pellet flux, however, because the majority of large (>1 mm) zooplankton were carnivorous species (78% carnivorous during the

Downloaded from https://academic.oup.com/plankt/advance-article/doi/10.1093/plankt/fbab001/6129944 by Florida State University Law Library user on 08 February 2021

day, 60% carnivorous at night) (Landry and Swalethorp, this issue). Both phaeopigment and chlorophyll flux then declined through the mesopelagic, with the Chl:Phaeo ratio also continuing to decline for three out of four cycles. These results suggest that the role of phytoplankton in sinking particles declines with increasing depth, while the role of fecal pellets generally increases, although most sinking carbon could not be identified from pigment signatures. Together with the results presented above, the changing character of flux with depth clearly indicates a system in which slowly sinking particles are rapidly consumed and or re-packaged multiple times as they sink into the mesopelagic.

The flux of phaeopigments out of the base of the EZ (64–283 μg m^{-2} d^{-1}) can also be compared to mesozooplankton grazing rates (217–803 μg m^{-2} d^{-1}) measured on our cruise by the gut pigment method (Landry and Swalethorp, this issue) to understand the potential remineralization of fecal pellets within the EZ. Across the four cycles on which pigment flux was measured, 29–61% of the pigment consumed by mesozooplankton exited the EZ. Only 16–46% of the chlorophyll consumed by mesozooplankton was caught in deep sediment traps at 231 m. These results suggest substantial remineralization of fecal pellets as they sink through the euphotic and twilight zones. High remineralization rates are likely driven by warm temperatures (enhanced microbial remineralization) and by comparatively low fecal pellet sinking rates that in turn reflect the predominantly small size of herbivorous zooplankton in the region and low abundance of phytoplankton with mineral tests that would increase fecal pellet density (Landry and Swalethorp, this issue; Selph *et al.*, this issue). These results show that efficient export of fecal pellets from the EZ should not be assumed, while the overall low grazing rates and low export of phaeopigments reflect a system with comparatively low mesozooplankton biomass (Shropshire *et al.*, 2020; Landry and Swalethorp, this issue; Shiroza *et al.*, this issue).

Comparison of GoM to other regions

The efficiency with which the BCP converts NPP into sinking particles and transports these particles into and through the mesopelagic is complicated by multiple intersecting physical, ecological and chemical interactions (Buesseler and Boyd, 2009; Burd and Jackson, 2009; Steinberg and Landry, 2017; Boyd *et al.*, 2019). Nevertheless, multiple empirical and mechanistic studies have attempted to relate export efficiency to simple ecosystem metrics, including temperature, NPP and surface chlorophyll (Laws *et al.*, 2000; Dunne *et al.*, 2005; Henson *et al.*, 2011). Early global meta-analyses suggested a positive correlation between export efficiency and ecosystem productivity (Eppley and Peterson, 1979; Laws *et al.*, 2000). However, studies focused on export variability within ecosystems (rather than across ecosystems) have found no correlation or an inverse relationship between export efficiency and NPP (Karl *et al.*, 1996; Michaels and Knap (1996); Maiti *et al.*, 2013; Kelly *et al.*, 2018). These relationships have been attributed, in part, to spatial or temporal mismatches between productivity and export (Benitez-Nelson *et al.*, 2001a; Kelly *et al.*, 2018; Laws and Maiti, 2019) or to food web ecological processes (Forest *et al.*, 2010; Le Moigne *et al.*, 2016). Nevertheless, substantial uncertainty remains. Process-oriented elucidation of the mechanisms driving variability in export efficiency is critical to quantifying the global magnitude of the BCP more accurately and to predicting its future responses to climate change.

Multiple studies spanning several seasons, sub-regions, and mesoscale features in the open-ocean GoM now give us the ability to generalize export patterns in the GoM (Guo *et al.*, 2002; Hung *et al.*, 2004, 2010; Maiti *et al.*, 2016). Results consistently show low export in the region. Maiti et al. (2016) measured an average of 2.7 mmol C m^{-2} d^{-1} in the northern GoM following the Deepwater Horizon Oil Spill. Average export in cold- and warm core rings were 5.2 and 6.0 mmol C m^{-2} d^{-1}, respectively (Hung *et al.*, 2004, 2010). In the present study, export at the euphotic-zone base ranged from 3.2 to 6.2 mmol C m^{-2} d^{-1}. These export values are slightly higher than estimates at oligotrophic time-series study sites in the Sargasso Sea and North Pacific Subtropical Gyre, despite the fact that NPP in the GoM studies was typically similar to, or lower than, average NPP at the time-series sites. Consequently, the GoM studies typically had higher EZ ratios in the range of 10–20% (Fig. 6a). Transfer efficiency through the mesopelagic appears to be similar in the GoM and the HOT and BATS time-series sites (Fig. 6b), leading to a slightly higher proportion of NPP being sequestered in the deep ocean GoM.

Notably, Maiti *et al.* (2016) is the only GoM study with low EZ ratios similar to the oligotrophic time-series sites. One possibility is that their NPP estimates were too high (they estimated NPP from satellite rather than *in situ* measurement). However, our *in situ* NPP measurements were not dissimilar from satellite estimates. Rather, the differences likely stem from season. The Maiti *et al.* (2016) study was conducted in March, at the end of the productive winter season; our study was conducted mostly in May, during the less productive summer season. Another distinct difference between the GoM studies is their positioning with respect to mesoscale features. The Hung *et al.* (2004, 2010) studies were conducted mostly within cyclonic or anti-cyclonic eddies. Maiti *et al.* (2016)

Downloaded from https://academic.oup.com/plankt/advance-article/doi/10.1093/plankt/fbab001/6129944 by Florida State University Law Library user on 08 February 2021

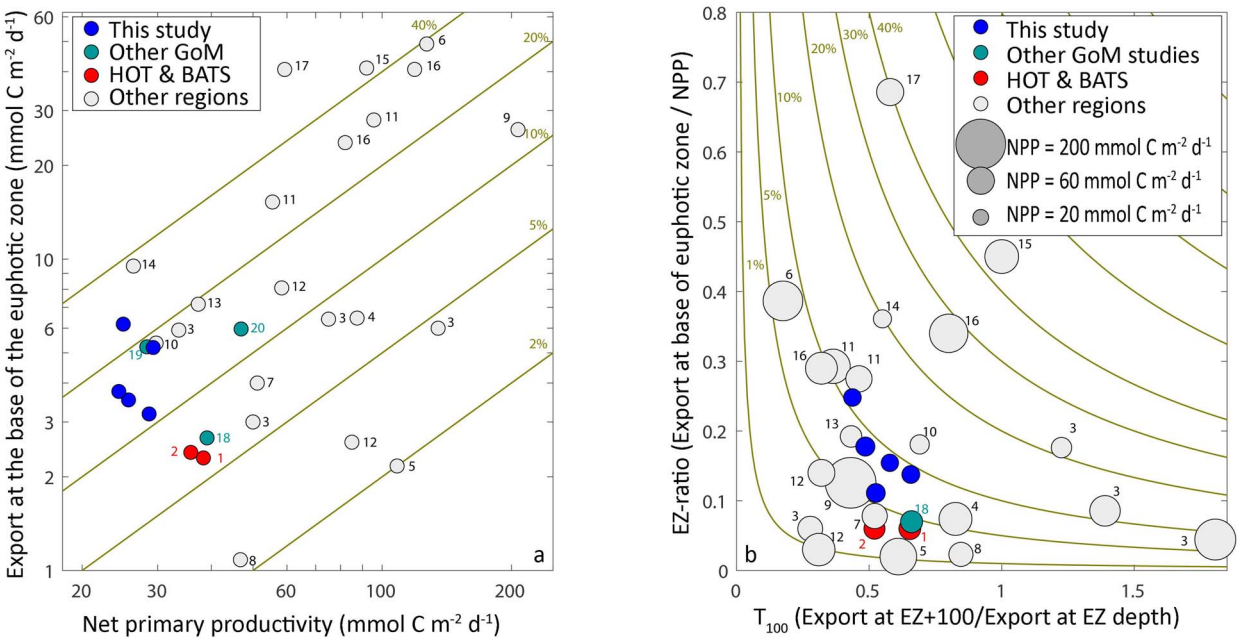

Fig. 6. Comparison of open-ocean GoM export efficiency to other regions. (**a**) EZ export plotted against NPP. Lines show EZ ratio values. (**b**) EZ ratio plotted against T_{100} (flux efficiency through the twilight zone). Solid lines show the proportion of NPP exported at least 100 m deeper than the base of the EZ (following Buesseler and Boyd, 2009; Buesseler *et al.*, 2020). With the exception of symbols for this study, all results are means from multiple trap deployments or ^{234}Th profiles in a specific region, biogeochemical province or mesoscale feature. [1]Subtropical Pacific average (Church *et al.*, 2013). [2]Sargasso Sea average (Lomas *et al.*, 2013). [3]Sargasso Sea eddies (Buesseler *et al.*, 2008a). [4]Costa Rica Dome (Stukel *et al.*, 2016). [5]Equatorial Pacific (Bacon *et al.*, 1996). [6]Tropical South Pacific, shelf (Black *et al.*, 2018). [7]Tropical South Pacific, offshore (Black *et al.*, 2018). [8]Tropical South Pacific, gyre (Black *et al.*, 2018). [9]California Current Ecosystem, coastal upwelling (Stukel and Barbeau, 2020). [10]California Current Ecosystem, offshore oligotrophic (Stukel and Barbeau, 2020). [11]California Current Ecosystem, frontal regions (Krause *et al.*, 2015; Stukel *et al.*, 2017). [12]Subarctic Pacific (Charette *et al.*, 1999). [13]Subarctic Pacific (Buesseler *et al.*, 2008b). [14]Spanish continental margin (Olli *et al.*, 2001). [15]North Atlantic Bloom (Buesseler *et al.*, 1992). [16]Southern Ocean (Buesseler *et al.*, 2003). [17]Barents Sea (Andreassen and Wassmann, 1998). [18]Northern GoM (Maiti *et al.*, 2016). [19]GoM cold-core rings (Hung *et al.*, 2004; Hung *et al.*, 2010). [20]GoM warm core rings (Hung *et al.*, 2004; Hung *et al.*, 2010).

sampled fixed locations relative to the Deepwater Horizon site. Our study targeted regions expected to have larval Atlantic bluefin tuna, which are more abundant in anti-cyclonic eddy boundaries (Muhling *et al.*, 2010; Domingues *et al.*, 2016). Disentangling these alternate potential drivers of intra-regional variability is not possible from the data currently available. Nevertheless, it is clear that despite very low NPP, the GoM can have moderate EZ ratios in May, higher than the average at HOT or BATS.

The GoM is not the only oligotrophic region with moderate EZ ratio. NPP and export are similar in offshore, oligotrophic regions of the California Current Ecosystem, on the continental shelf off of northwest Spain, and at station K2 in the subarctic Pacific (Fig. 6a). Comparing across multiple regions in Fig. 6, there is no strong relationship between export efficiency and EZ ratio. Rather, high and low EZ ratios are found in both high- and low-productivity regimes. Since we plotted only means of multiple sediment trap or ^{234}Th export efficiency values in Fig. 6 (except for all data points from this study), we do not suspect that the lack of correlation between export efficiency and NPP is due to a temporal mismatch between export and production (as has been hypothesized to explain intra-regional variability). Rather, we believe that NPP is not a strong predictor of export efficiency and that the EZ ratio must be set by other food web, chemical or physical properties. Notably, our cruise results show that the GoM is a picoplankton-dominated ecosystem, with comparatively low mesozooplankton grazing, and a strong microbial loop (Landry *et al.*, this issue; Selph *et al.*, this issue). This trophic structure, combined with very warm GoM temperatures, would generally suggest a high-recycling, low-export condition. However, our study site had approximately equal contributions of autotrophic eukaryotes and *Prochlorococcus* to phytoplankton biomass, while HOT and BATS are typically *Prochlorococcus* dominated (Selph *et al.*, this issue). Relative to NPP, the GoM also has higher mesozooplankton biomass than HOT and BATS (Landry and Swalethorp, this issue). Both of these food-web differences could lead to more-efficient carbon export, highlighting the potential for trophic ecology to modify NPP to export relationships. An alternate (or complementary) hypothesis for higher export efficiency

Downloaded from https://academic.oup.com/plankt/advance-article/doi/10.1093/plankt/fbab001/6129944 by Florida State University Law Library user on 08 February 2021

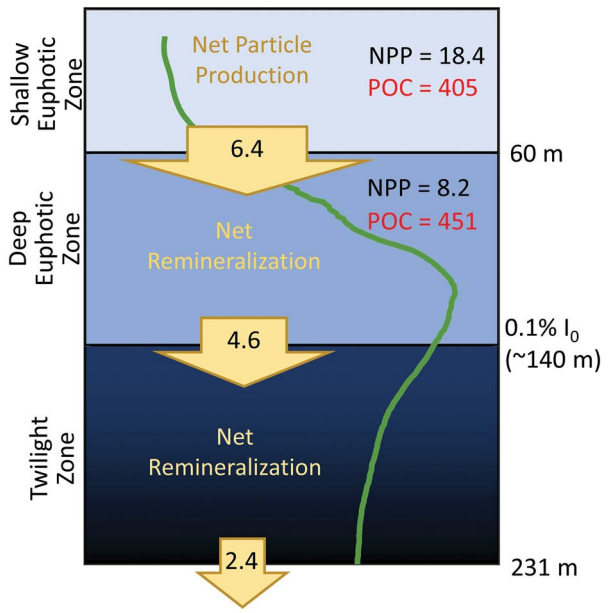

Fig. 7. Average carbon budget for the shallow (0–60 m) and deep (60 m to 0.1% incident irradiance) EZ, as well as the twilight zone (~140–231 m). Black values are fluxes of NPP (mmol C m^{-2} d^{-1}) and sinking particle flux (arrows, mmol C m^{-2} d^{-1}), while red values are POC standing stock (mmol C m^{-2}). The green trace line is the average chlorophyll profile, with mean values of 0.1 μg Chl *a* L^{-1} in the shallow EZ and 0.41 μg Chl *a* L^{-1} at the deep chlorophyll maximum.

in this region relates to the high eddy kinetic energy and strong lateral gradients in the GoM (Zhong and Bracco, 2013; Cardona and Bracco, 2016; Gomez *et al.*, 2018). Meso- and submesoscale processes may transport non-living organic matter and plankton from productive areas to the oligotrophic central GoM, where this excess production supplements locally derived particles and strengthens the efficiency of the biological pump (Kelly *et al.*, in review; Landry and Swalethorp, this issue).

CONCLUSION

Despite very deep DCM and euphotic depths ranging from 128–150 m, net particle production in the oceanic GoM is mostly limited to the upper EZ (Fig. 7). Nevertheless, there is substantial modification of sinking particles as they transit the euphotic and twilight zones, indicating particle destruction, new particle creation and multiple particle transformations. Particles sinking from the upper to the lower EZ were mostly non-pigmented, but contained substantially more chlorophyll (indicative of fresh phytoplankton) than phaeopigments (indicative of herbivore fecal pellets). At deeper depths, however, particles contained mostly phaeopigments, indicating that fecal pellets were more important to export from the EZ than fresh phytoplankton. Shifts in elemental and isotopic composition of sinking particles give further evidence of particle transformation during transit to depth.

Comparison to contemporaneous NPP measurements, and to similar measurements from other GoM studies and regions, show that our study region has moderate export efficiency from the EZ and transfer efficiency through the mesopelagic. Thus, despite very low primary productivity, the open-ocean GoM sequesters a proportion of NPP similar to many more productive ecosystems. This suggests that the BCP can be efficient even in warm, stratified, low-biomass regions. We suspect that the high mesoscale kinetic energy and lateral processes in the GoM contributes to this higher-than-expected sequestration potential.

DATA ARCHIVING

Data presented here have been submitted to the National Oceanic and Atmospheric Administration's (NOAA) National Centers for Environmental Information (NCEI) data repository and are also be archived at BCO-DMO (Biological and Chemical Oceanography Data Management Office) site https://www.bco-dmo.org/program/819631.

ACKNOWLEDGEMENTS

We are very gratefully to our many colleagues within the BLOOFINZ-GoM project and especially thank John Lamkin and Trika Gerard (project leads) and Estrella Malca (chief scientist on NF17 cruise).

FUNDING

National Science Foundation Biological Oceanography (grant OCE-1851347); a National Oceanic and Atmospheric Administration's RESTORE Program Grant (Project Title: Effects of nitrogen sources and plankton food-web dynamics on habitat quality for the larvae of Atlantic bluefin tuna in the GoM) under federal funding opportunity NOAA-NOS-NCCOS-2017-2004875; including NOAA JIMAR Cooperative Agreement (award #NA16NMF4320058); NOAA CIMAS Cooperative Agreement (award #NA15OAR4320064); NOAA CIMEAS Cooperative Agreement (award #NA15OAR4320071). https://restoreactscienceprogram.noaa.gov/funded-projects/bluefin-tuna-larvae.

REFERENCES

Andreassen, I. J. and Wassmann, P. (1998) Vertical flux of phytoplankton and particulate biogenic matter in the marginal ice zone of the Barents Sea in May 1993. *Mar. Ecol. Prog. Ser.*, **170**, 1–14.

Archibald, K. M., Siegel, D. A. and Doney, S. C. (2019) Modeling the impact of zooplankton diel vertical migration on the carbon export flux of the biological pump. *Global Biogeochem. Cycles*, **33**, 181–199.

Downloaded from https://academic.oup.com/plankt/advance-article/doi/10.1093/plankt/fbab001/6129944 by Florida State University Law Library user on 08 February 2021

Armstrong, R. A., Lee, C., Hedges, J. I., Honjo, S. and Wakeham, S. G. (2002) A new, mechanistic model for organic carbon fluxes in the ocean based on the quantitative association of POC with ballast minerals. *Deep-Sea Res. II*, **49**, 219–236.

Bacon, M. P., Cochran, J. K., Hirschberg, D., Hammar, T. R. and Fleer, A. P. (1996) Export flux of carbon at the equator during the EqPac time-series cruises estimated from Th-234 measurements. *Deep-Sea Res. II*, **43**, 1133–1153.

Baker, C. A., Estapa, M. L., Iversen, M., Lampitt, R. and Buesseler, K. (2020) Are all sediment traps created equal? An intercomparison study of carbon export methodologies at the PAP-SO site. *Prog. Oceanogr.*, **184**, 102317.

Baker, E. T., Milburn, H. B. and Tennant, D. A. (1988) Field assessment of sediment trap efficiency under varying flow conditions. *J. Mar. Res.*, **46**, 573–592.

Belcher, A., Iversen, M., Manno, C., Henson, S. A., Tarling, G. A. and Sanders, R. (2016) The role of particle associated microbes in remineralization of fecal pellets in the upper mesopelagic of the Scotia Sea, Antarctica. *Limnol. Oceanogr.*, **61**, 1049–1064.

Benitez-Nelson, C. R., Buesseler, K. O., Karl, D. M. and Andrews, J. (2001a) A time-series study of particulate matter export in the North Pacific subtropical gyre based on Th-234: U-238 disequilibrium. *Deep-Sea Res. I*, **48**, 2595–2611.

Benitez-Nelson, C. R., Buesseler, K. O., Van Der Loeff, M. R., Andrews, J., Ball, L., Crossin, G. and Charette, M. A. (2001b) Testing a new small-volume technique for determining Th-234 in seawater. *J. Radioanal. Nucl. Chem.*, **248**, 795–799.

Biggs, D. C. (1992) Nutrients, plankton, and productivity in a warm-core ring in the western Gulf of Mexico. *J. Geophys. Res. Oceans*, **97**, 2143–2154.

Biggs, D. C., Hu, C. and Müller-Karger, F. E. (2008) Remotely sensed sea-surface chlorophyll and POC flux at deep Gulf of Mexico benthos sampling stations. *Deep-Sea Res. II*, **55**, 2555–2562.

Black, E. E., Buesseler, K. O., Pike, S. M. and Lam, P. J. (2018) ^{234}Th as a tracer of particulate export and remineralization in the southeastern tropical Pacific. *Mar. Chem.*, **201**, 35–50.

Boyd, P. W., Claustre, H., Levy, M., Siegel, D. A. and Weber, T. (2019) Multi-faceted particle pumps drive carbon sequestration in the ocean. *Nature*, **568**, 327–335.

Buesseler, K. O., Antia, A. N., Chen, M., Fowler, S. W., Gardner, W. D., Gustafsson, O., Harada, K., Michaels, A. F. *et al.* (2007) An assessment of the use of sediment traps for estimating upper ocean particle fluxes. *J. Mar. Res.*, **65**, 345–416.

Buesseler, K. O., Bacon, M. P., Cochran, J. K. and Livingston, H. D. (1992) Carbon and nitrogen export during the JGOFS North Atlantic bloom experiment estimated from ^{234}Th:^{238}U disequilibria. *Deep-Sea Res.*, **39**, 1115–1137.

Buesseler, K. O., Barber, R. T., Dickson, M.-L., Hiscock, M. R., Moore, J. K. and Sambrotto, R. (2003) The effect of marginal ice-edge dynamics on production and export in the Southern Ocean along 170 W. *Deep-Sea Res. II*, **50**, 579–603.

Buesseler, K. O. and Boyd, P. W. (2009) Shedding light on processes that control particle export and flux attenuation in the twilight zone of the open ocean. *Limnol. Oceanogr.*, **54**, 1210–1232.

Buesseler, K. O., Boyd, P. W., Black, E. E. and Siegel, D. A. (2020) Metrics that matter for assessing the ocean biological carbon pump. *Proc. Natl. Acad. Sci. USA.*, **117**, 9679–9687.

Buesseler, K. O., Lamborg, C., Cai, P., Escoube, R., Johnson, R., Pike, S., Masque, P., Mcgillicuddy, D. *et al.* (2008a) Particle fluxes associated with mesoscale eddies in the Sargasso Sea. *Deep-Sea Res. II*, **55**, 1426–1444.

Buesseler, K. O., Trull, T. W., Steinber, D. K., Silver, M. W., Siegel, D. A., Saitoh, S. I., Lamborg, C. H., Lam, P. J. *et al.* (2008b) VERTIGO (VERtical transport in the Global Ocean): a study of particle sources and flux attenuation in the North Pacific. *Deep-Sea Res. II*, **55**, 1522–1539.

Burd, A. B. and Jackson, G. A. (2009) Particle aggregation. *Ann. Rev. Mar. Sci.*, **1**, 65–90.

Cardona, Y. and Bracco, A. (2016) Predictability of mesoscale circulation throughout the water column in the Gulf of Mexico. *Deep-Sea Res. II*, **129**, 332–349.

Carlson, C. A., Ducklow, H. W. and Michaels, A. F. (1994) Annual flux of dissolved organic carbon from the euphotic zone in the northwestern Sargasso Sea. *Nature*, **371**, 405–408.

Chanton, J., Giering, S. L., Bosman, S. H., Rogers, K. L., Sweet, J., Asper, V., Diercks, A.-R. and Passow, U. (2018) Isotopic composition of sinking particles: oil effects, recovery and baselines in the Gulf of Mexico, 2010-2015. *Elementa: Science of the Anthropocene*, **6**, 43.

Charette, M. A., Moran, S. B. and Bishop, J. K. (1999) ^{234}Th as a tracer of particulate organic carbon export in the subarctic northeast Pacific Ocean. *Deep Sea Research II*, **46**, 2833–2861.

Church, M. J., Lomas, M. W. and Muller-Karger, F. (2013) Sea change: charting the course for biogeochemical ocean time-series research in a new millennium. *Deep-Sea Res. II*, **93**, 2–15.

Cornic, M., Smith, B. L., Kitchens, L. L., Bremer, J. R. A. and Rooker, J. R. (2018) Abundance and habitat associations of tuna larvae in the surface water of the Gulf of Mexico. *Hydrobiologia*, **806**, 29–46.

Domingues, R., Goni, G., Bringas, F., Muhling, B., Lindo-Atichati, D. and Walter, J. (2016) Variability of preferred environmental conditions for Atlantic bluefin tuna (*Thunnus thynnus*) larvae in the Gulf of Mexico during 1993–2011. *Fish. Oceanogr.*, **25**, 320–336.

Ducklow, H. W., Steinberg, D. K. and Buesseler, K. O. (2001) Upper Ocean carbon export and the biological pump. *Oceanography*, **14**, 50–58.

Dunne, J. P., Armstrong, R. A., Gnanadesikan, A. and Sarmiento, J. L. (2005) Empirical and mechanistic models for the particle export ratio. *Global Biogeochem. Cycles*, **19**, GB4026.

Eppley, R. W. and Peterson, B. J. (1979) Particulate organic matter flux and planktonic new production in the deep ocean. *Nature*, **282**, 677–680.

Estapa, M. L., Siegel, D. A., Buesseler, K. O., Stanley, R. H. R., Lomas, M. W. and Nelson, N. B. (2015) Decoupling of net community and export production on submesoscales. *Global Biogeochem. Cycles*, **29**, 1266–1282.

Forest, A., Wassmann, P., Slagstad, D., Bauerfeind, E., Nöthig, E.-M. and Klages, M. (2010) Relationships between primary production and vertical particle export at the Atlantic-Arctic boundary (Fram Strait, HAUSGARTEN). *Polar Biol.*, **33**, 1733–1746.

Gargett, A. and Garner, T. (2008) Determining Thorpe scales from ship-lowered CTD density profiles. *J. Atmos. Oceanic Tech.*, **25**, 1657–1670.

Gerard, T., Lamkin, R. T., Kelly, T. B., Knapp, A. N., Laiz-Carrión, R., Malca, E., Selph, K. E., Stukel, M. R. *et al.* this issueBluefin larvae in Oligotrophic Ocean Foodwebs, investigations of nutrients to zooplankton: overview of the BLOOFINZ-Gulf of Mexico program. *J. Plankton Res.*.

Downloaded from https://academic.oup.com/plankt/advance-article/doi/10.1093/plankt/fbab001/6129944 by Florida State University Law Library user on 08 February 2021

Gomez, F. A., Lee, S.-K., Liu, Y., Hernandez, F. J. Jr., Muller-Karger, F. E. and Lamkin, J. T. (2018) Seasonal patterns in phytoplankton biomass across the northern and deep Gulf of Mexico: a numerical model study. *Biogeosciences*, **15**, 3561–3576.

Gorsky, G. and Fenaux, R. (1998) The role of Appendicularia in marine food webs. In Bone (ed.) *The Biology of Pelagic Tunicates*. pp. 161–169.

Green, R. E., Bower, A. S. and Lugo-Fernandez, A. (2014) First autonomous bio-optical profiling float in the Gulf of Mexico reveals dynamic biogeochemistry in deep waters. *PLoS One*, **9**, e101658.

Guo, L., Hung, C.-C., Santschi, P. H. and Walsh, I. D. (2002) ^{234}Th scavenging and its relationship to acid polysaccharide abundance in the Gulf of Mexico. *Mar. Chem.*, **78**, 103–119.

Habtes, S., Muller-Karger, F. E., Roffer, M. A., Lamkin, J. T. and Muhling, B. A. (2014) A comparison of sampling methods for larvae of medium and large epipelagic fish species during spring SEAMAP ichthyoplankton surveys in the Gulf of Mexico. *Limnol. Oceanogr. Meth.*, **12**, 86–101.

Hansell, D. A., Carlson, C. A., Repeta, D. J. and Schlitzer, R. (2009) Dissolved organic matter in the ocean: a controversy stimulates new insights. *Oceanography*, **22**, 202–211.

Henson, S. A., Sanders, R., Madsen, E., Morris, P. J., Moigne, F. and Quartly, G. D. (2011) A reduced estimate of the strength of the ocean's biological carbon pump. *Geophys. Res. Lett.*, **38**, L04606.

Hung, C.-C., Guo, L., Roberts, K. A. and Santschi, P. H. (2004) Upper Ocean carbon flux determined by the ^{234}Th approach and sediment traps using size-fractionated POC and ^{234}Th data from the Gulf of Mexico. *Geochem. J.*, **38**, 601–611.

Hung, C. C., Xu, C., Santschi, P. H., Zhang, S. J., Schwehr, K. A., Quigg, A., Guo, L. D., Gong, G. C. *et al.* (2010) Comparative evaluation of sediment trap and ^{234}Th-derived POC fluxes from the upper oligotrophic waters of the Gulf of Mexico and the subtropical northwestern Pacific Ocean. *Mar. Chem.*, **121**, 132–144.

Kahru, M., Goericke, R., Kelly, T. B. and Stukel, M. R. (2019) Satellite estimation of carbon export by sinking particles in the California current calibrated with sediment trap data. *Deep-Sea Res. II*, **173**, 104639.

Karl, D. M., Christian, J. R., Dore, J. E., Hebel, D. V., Letelier, R. M., Tupas, L. M. and Winn, C. D. (1996) Seasonal and interannual variability in primary production and particle flux at station ALOHA. *Deep-Sea Res. II*, **43**, 539–568.

Kelly, T. B., Goericke, R., Kahru, M., Song, H. and Stukel, M. R. (2018) CCE II: spatial and interannual variability in export efficiency and the biological pump in an eastern boundary current upwelling system with substantial lateral advection. *Deep-Sea Res. I*, **140**, 14–25.

Kelly, T. B., Landry, M. R., Selph, K. E., Knapp, A. N., Swalethorp, R. and Stukel, M. R. (in review)Lateral advection supports nitrogen export in the oligotrophic ecosystem of the open-ocean Gulf of Mexico. *Nat. Commun.*

Knapp, A. N., Thomas, R., Stukel, M. R., Kelly, T. B., Landry, M. R., Selph, K. E., Malca, E., Gerard, T. *et al.* this issueConstraining the sources of nitrogen fueling phytoplankton and food webs in the Gulf of Mexico using nitrogen isotope budgets. *J. Plankton Res.*

Knauer, G. A., Martin, J. H. and Bruland, K. W. (1979) Fluxes of particulate carbon, nitrogen, and phosphorus in the upper water column of the Northeast Pacific. *Deep-Sea Res.*, **26**, 97–108.

Krause, J. W., Brzezinski, M. A., Goericke, R., Landry, M. R., Ohman, M. D., Stukel, M. R. and Taylor, A. G. (2015) Variability in diatom contributions to biomass, organic matter production and export across a frontal gradient in the California current ecosystem. *J. Geophys. Res. Oceans*, **120**, 1032–1047.

Kwon, E. Y., Primeau, F. and Sarmiento, J. L. (2009) The impact of remineralization depth on the air-sea carbon balance. *Nat. Geosci.*, **2**, 630–635.

Landry, M. R., Ohman, M. D., Goericke, R., Stukel, M. R. and Tsyrklevich, K. (2009) Lagrangian studies of phytoplankton growth and grazing relationships in a coastal upwelling ecosystem off Southern California. *Prog. Oceanogr.*, **83**, 208–216.

Landry, M. R., Selph, K. E., Stukel, M. R., Swalethorp, R., Kelly, T. B., Beatty, J. L. and Quackenbush, C. R. this issueMicrobial food web dynamics in the oceanic Gulf of Mexico. *J. Plankton Res.*.

Landry, M. R. and Swalethorp, R. (this issue) Mesozooplankton biomass, grazing and trophic structure in the bluefin tuna spawning area of the oceanic Gulf of Mexico. *J. Plankton Res.*.

Laws, E. A., D'sa, E. and Naik, P. (2011) Simple equations to estimate ratios of new or export production to total production from satellite-derived estimates of sea surface temperature and primary production. *Limnol. Oceanogr. Meth.*, **9**, 593–601.

Laws, E. A., Falkowski, P. G., Smith, W. O., Ducklow, H. and Mccarthy, J. J. (2000) Temperature effects on export production in the open ocean. *Global Biogeochem. Cycles*, **14**, 1231–1246.

Laws, E. A. and Maiti, K. (2019) The relationship between primary production and export production in the ocean: effects of time lags and temporal variability. *Deep Sea Res. I*, **148**, 100–107.

Le Moigne, F. A., Henson, S. A., Cavan, E., Georges, C., Pabortsava, K., Achterberg, E. P., Ceballos-Romero, E., Zubkov, M. *et al.* (2016) What causes the inverse relationship between primary production and export efficiency in the Southern Ocean? *Geophys. Res. Lett.*, **43**, 4457–4466.

Lomas, M. W., Bates, N. R., Johnson, R. J., Knap, A. H., Steinberg, D. K. and Carlson, C. A. (2013) Two decades and counting: 24-years of sustained open ocean biogeochemical measurements in the Sargasso Sea. *Deep-Sea Res. II*, **93**, 16–32.

Maiti, K., Bosu, S., D'sa, E. J., Adhikari, P. L., Sutor, M. and Longnecker, K. (2016) Export fluxes in northern Gulf of Mexico-comparative evaluation of direct, indirect and satellite-based estimates. *Mar. Chem.*, **184**, 60–77.

Maiti, K., Charette, M. A., Buesseler, K. O. and Kahru, M. (2013) An inverse relationship between production and export efficiency in the Southern Ocean. *Geophys. Res. Lett.*, **40**, 1557–1561.

Marsay, C. M., Sanders, R. J., Henson, S. A., Pabortsava, K., Achterberg, E. P. and Lampitt, R. S. (2015) Attenuation of sinking particulate organic carbon flux through the mesopelagic ocean. *Proc. Natl. Acad. Sci. USA*, **112**, 1089–1094.

Martin, J. H., Knauer, G. A., Karl, D. M. and Broenkow, W. W. (1987) Vertex: carbon cycling in the Northeast Pacific. *Deep-Sea Res.*, **34**, 267–285.

McDonnell, A. M. P. and Buesseler, K. O. (2010) Variability in the average sinking velocity of marine particles. *Limnol. Oceanogr.*, **55**, 2085–2096.

Menden-Deuer, S. and Lessard, E. J. (2000) Carbon to volume relationships for dinoflagellates, diatoms, and other protist plankton. *Limnol. Oceanogr.*, **45**, 569–579.

Michaels, A. F., , and Knap, A. H. (1996) Overview of the US JGOFS Bermuda Atlantic Time-series Study and the Hydrostation S program. *Deep-Sea Res. II*, **43**, 157–198.

Downloaded from https://academic.oup.com/plankt/advance-article/doi/10.1093/plankt/fbab001/6129944 by Florida State University Law Library user on 08 February 2021

Muhling, B. A., Lamkin, J. T. and Roffer, M. A. (2010) Predicting the occurrence of Atlantic bluefin tuna (*Thunnus thynnus*) larvae in the northern Gulf of Mexico: building a classification model from archival data. *Fish. Oceanogr.*, **19**, 526–539.

Oey, L., Ezer, T. and Lee, H. (2005) Loop current, rings and related circulation in the Gulf of Mexico: a review of numerical models and future challenges. *Geophysical Monograph-AGU*, **161**, 31–56.

Olli, K., Riser, C. W., Wassmann, P., Ratkova, T., Arashkevich, E. and Pasternak, A. (2001) Vertical flux of biogenic matter during a Lagrangian study off the NW Spanish continental margin. *Progress in Oceanography*, **51**, 443–466.

Omand, M. M., D'asaro, E. A., Lee, C. M., Perry, M. J., Briggs, N., Cetinić, I. and Mahadevan, A. (2015) Eddy-driven subduction exports particulate organic carbon from the spring bloom. *Science*, **348**, 222–225.

Owens, S. A., Buesseler, K. O. and Sims, K. W. W. (2011) Re-evaluating the ^{238}U-salinity relationship in seawater: implications for the ^{238}U-^{234}Th disequilibrium method. *Mar. Chem.*, **127**, 31–39.

Passow, U. (2016) Formation of rapidly-sinking, oil-associated marine snow. *Deep-Sea Res. II*, **129**, 232–240.

Passow, U., Ziervogel, K., Asper, V. and Diercks, A. (2012) Marine snow formation in the aftermath of the Deepwater horizon oil spill in the Gulf of Mexico. *Environ. Res. Lett.*, **7**, 035301.

Pike, S. M., Buesseler, K. O., Andrews, J. and Savoye, N. (2005) Quantification of ^{234}Th recovery in small volume sea water samples by inductively coupled plasma-mass spectrometry. *J. Radioanal. Nucl. Chem.*, **263**, 355–360.

Rooker, J. R., Simms, J. R., Wells, R. D., Holt, S. A., Holt, G. J., Graves, J. E. and Furey, N. B. (2012) Distribution and habitat associations of billfish and swordfish larvae across mesoscale features in the Gulf of Mexico. *PLoS One*, **7**, e34180.

Savoye, N., Benitez-Nelson, C., Burd, A. B., Cochran, J. K., Charette, M., Buesseler, K. O., Jackson, G. A., Roy-Barman, M. *et al.* (2006) ^{234}Th sorption and export models in the water column: a review. *Mar. Chem.*, **100**, 234–249.

Selph, K. E., Landry, M. R., Taylor, A. G., Yang, E. J., Measures, C. I., Yang, J. J., Stukel, M. R., Christenson, S. *et al.* (2011) Spatially-resolved taxon-specific phytoplankton production and grazing dynamics in relation to iron distributions in the equatorial Pacific between 110 and 140°W. *Deep-Sea Res. II*, **58**, 358–377.

Selph, K. E., Swalethorp, R., Stukel, M. R., Kelly, T. B., Knapp, A. N., Fleming, K., Hernandez, T. and Landry, M. R. this issuePhytoplankton community composition and biomass in the oligotrophic Gulf of Mexico. *J. Plankton Res.*.

Shiroza, A., Malca, E., Lamkin, J. T., Gerard, T., Landry, M. R., Stukel, M. R., Laiz-Carrión, R. and Swalethorp, R. (this issue) active prey selection in developing larvae of Atlantic bluefin tuna (*Thunnus thynnus*) in spawning grounds of the Gulf of Mexico. *J. Plankton Res.*.

Shropshire, T. A., Morey, S. L., Chassignet, E. P., Bozec, A., Coles, V. J., Landry, M. R., Swalethorp, R., Zapfe, G. *et al.* (2020) Quantifying spatiotemporal variability in zooplankton dynamics in the Gulf of Mexico with a physical-biogeochemical model. *Biogeosciences*, **17**, 3385–3407.

Siegel, D. A., Buesseler, K. O., Behrenfeld, M. J., Benitez-Nelson, C. R., Boss, E., Brzezinski, M. A., Burd, A., Carlson, C. A. *et al.* (2016) Prediction of the export and fate of global ocean net primary production: the EXPORTS science plan. *Front. Mar. Sci.*, **3**, 22.

Siegel, D. A., Buesseler, K. O., Doney, S. C., Sailley, S. F., Behrenfeld, M. J. and Boyd, P. W. (2014) Global assessment of ocean carbon export by combining satellite observations and food-web models. *Global Biogeochem. Cycles*, **28**, 181–196.

Steinberg, D. K., Carlson, C. A., Bates, N. R., Goldthwait, S. A., Madin, L. P. and Michaels, A. F. (2000) Zooplankton vertical migration and the active transport of dissolved organic and inorganic carbon in the Sargasso Sea. *Deep-Sea Res. I*, **47**, 137–158.

Steinberg, D. K. and Landry, M. R. (2017) Zooplankton and the ocean carbon cycle. *Ann. Rev. Mar. Sci.*, **9**, 413–444.

Steinberg, D. K., Van Mooy, B. A. S., Buesseler, K. O., Boyd, P. W., Kobari, T. and Karl, D. M. (2008) Bacterial vs. zooplankton control of sinking particle flux in the ocean's twilight zone. *Limnol. Oceanogr.*, **53**, 1327–1338.

Strickland, J. D. and Parsons, T. R. (1972) A practical handbook of seawater analysis, second ed. *Bull. Fish. Res. Board Can.*, **167**., 201–204

Stukel, M. R., Aluwihare, L. I., Barbeau, K. A., Chekalyuk, A. M., Goericke, R., Miller, A. J., Ohman, M. D., Ruacho, A. *et al.* (2017) Mesoscale Ocean fronts enhance carbon export due to gravitational sinking and subduction. *Proc. Natl. Acad. Sci. USA*, **114**, 1252–1257.

Stukel, M. R. and Barbeau, K. A. (2020) Investigating the nutrient landscape in a coastal upwelling region and its relationship to the biological carbon pump. *Geophys. Res. Lett.*, **47**, e2020GL087351.

Stukel, M. R., Benitez-Nelson, C., Décima, M., Taylor, A. G., Buchwald, C. and Landry, M. R. (2016) The biological pump in the Costa Rica dome: an open ocean upwelling system with high new production and low export. *J. Plankton Res.*, **38**, 348–365.

Stukel, M. R., Gerard, T., Kelly, T. B., Knapp, A. N., Laiz-Carrión, R., Lamkin, J. T., Landry, M. R., Malca, E. *et al.* this issuePlankton food webs of the Gulf of Mexico spawning grounds of Atlantic Bluefin tuna. *J. Plankton Res.*.

Stukel, M. R., Kahru, M., Benitez-Nelson, C. R., Decima, M., Goericke, R., Landry, M. R. and Ohman, M. D. (2015) Using Lagrangian-based process studies to test satellite algorithms of vertical carbon flux in the eastern North Pacific Ocean. *J. Geophys. Res. Oceans*, **120**, 7208–7222.

Stukel, M. R., Kelly, T. B., Aluwihare, L. I., Barbeau, K. A., Goericke, R., Krause, J. W., Landry, M. R. and Ohman, M. D. (2019a) The carbon:^{234}Thorium ratios of sinking particles in the California current ecosystem 1: relationships with plankton ecosystem dynamics. *Mar. Chem.*, **212**, 1–15.

Stukel, M. R., Ohman, M. D., Kelly, T. B. and Biard, T. (2019b) The roles of filter-feeding and flux-feeding zooplankton as gatekeepers of particle flux into the mesopelagic ocean. *Front. Mar. Sci.*, **6**, 397.

Stukel, M. R., Song, H., Goericke, R. and Miller, A. J. (2018) The role of subduction and gravitational sinking in particle export, carbon sequestration, and the remineralization length scale in the California current ecosystem. *Limnol. Oceanogr.*, **63**, 363–383.

Taylor, A. G., Landry, M. R., Selph, K. E. and Wokuluk, J. J. (2015) Temporal and spatial patterns of microbial community biomass and composition in the Southern California current ecosystem. *Deep-Sea Res. II*, **112**, 117–128.

Trull, T. W., Bray, S. G., Buesseler, K. O., Lamborg, C. H., Manganini, S., Moy, C. and Valdes, J. (2008) In situ measurement of mesopelagic particle sinking rates and the control of carbon transfer to the ocean interior during the vertical flux in the Global Ocean (VERTIGO) voyages in the North Pacific. *Deep-Sea Res. II*, **55**, 1684–1695.

Downloaded from https://academic.oup.com/plankt/advance-article/doi/10.1093/plankt/fbab001/6129944 by Florida State University Law Library user on 08 February 2021

Turner, J. T. (2015) Zooplankton fecal pellets, marine snow, phytodetritus and the ocean's biological pump. *Prog. Oceanogr.*, **130**, 205–248.

Volk, T. and Hoffert, M. I. (1985) Ocean carbon pumps: Analysis of relative strengths and efficiencies in ocean-driven atmospheric CO_2 changes. In Sundquist, E. T. and Broeker, W. S. (eds.), *The Carbon Cycle and Atmospheric CO_2: Natural Variations Archean to Present*, American Geophysical Union, Washington, D. C, pp. 99–110.

Yingling, N., Kelly, T. B., Selph, K. E., Landry, M. R., Knapp, A. N., Kranz, S. A. and Stukel, M. R. this issueTaxon-specific phytoplankton growth, nutrient limitation, and light limitation in the oligotrophic Gulf of Mexico. *J. Plankton Res.*.

Zhong, Y. S. and Bracco, A. (2013) Submesoscale impacts on horizontal and vertical transport in the Gulf of Mexico. *J. Geophys. Res. Oceans*, **118**, 5651–5668.

Downloaded from https://academic.oup.com/plankt/advance-article/doi/10.1093/plankt/fbab001/6129944 by Florida State University Law Library user on 08 February 2021